Veterinary Research

RESEARCH

Open Access

Functional and lncRNA changes in ovine blood monocytes and derived macrophages following paratuberculosis vaccination

Pedro Mendívil[1,2†], Noive Arteche-Villasol[2*†], Natalia Elguezabal[3], Maitane Mugica-Unamuno[3], Elena Molina[3], Ignacio Fernández[2], Miguel Criado[2], Marta Silva[2], Daniel Gutiérrez-Expósito[1,2], Julio Benavides[2] and Miguel Fernández[1]

Abstract

Vaccination is central to control paratuberculosis in ruminants. Commercial vaccines such as Gudair®, although not fully preventing infection, reduce clinical signs and faecal shedding. Nevertheless, their protective immunological mechanisms remain unclear. This study evaluated the effect of Gudair® vaccination on mononuclear phagocyte function in sheep (*Ovis aries*) and correlated it with their long non-coding RNA (lncRNA) expression. Ten Assaf lambs were divided into vaccinated ($n = 5$) and non-vaccinated ($n = 5$) groups. Peripheral blood was collected before vaccination and at 30-, 60- and 90-days post-vaccination (dpv) to assess antigen-specific IFN-γ and antibody responses. Phagocytosis and reactive oxygen species (ROS) production were evaluated in the monocyte fraction following in vitro *Mycobacterium avium* subsp. *paratuberculosis* (Map) infection of whole blood. At 90 dpv, monocytes were also isolated from peripheral blood to generate ovine monocyte-derived macrophages (OvMDMs) to assess Map phagocytosis and intracellular survival and lncRNAs expression analysis by RNA-seq. Vaccination induced increased IFN-γ and anti-Map antibody responses over time. Monocytes from vaccinated lambs showed significantly higher ROS production at 90 dpv ($p < 0.05$), whereas phagocytosis did not differ between groups. No significant differences were observed in OvMDMs regarding Map phagocytosis or bacterial survival. Transcriptome analysis of monocytes at 90 dpv identified 6854 lncRNAs (4719 annotated and 2135 novel), of which four were differentially expressed between groups. Cis- and trans-based computational analyses identified potential associations with genes involved in immune-related pathways. These findings improve our understanding of the innate immune responses induced by paratuberculosis vaccination and identify candidate lncRNAs for further investigation in vaccine-induced immunity.

Keywords Innate immunity, non-coding RNAs, ex vivo, vaccination, immunomodulation

Handling editor: Kate Sutton

†Pedro Mendívil and Noive Arteche-Villasol have contributed equally to this work.

*Correspondence:
Noive Arteche-Villasol
noive.arteche@csic.es
Full list of author information is available at the end of the article

© The Author(s) 2026. **Open Access** This article is licensed under a Creative Commons Attribution 4.0 International License, which permits use, sharing, adaptation, distribution and reproduction in any medium or format, as long as you give appropriate credit to the original author(s) and the source, provide a link to the Creative Commons licence, and indicate if changes were made. The images or other third party material in this article are included in the article's Creative Commons licence, unless indicated otherwise in a credit line to the material. If material is not included in the article's Creative Commons licence and your intended use is not permitted by statutory regulation or exceeds the permitted use, you will need to obtain permission directly from the copyright holder. To view a copy of this licence, visit http://creativecommons.org/licenses/by/4.0/. The Creative Commons Public Domain Dedication waiver (http://creativecommons.org/publicdomain/zero/1.0/) applies to the data made available in this article, unless otherwise stated in a credit line to the data.

Introduction

Paratuberculosis is a chronic granulomatous enteritis of ruminants caused by *Mycobacterium avium* subsp. *paratuberculosis* (Map), leading to progressive weight loss and reduced productivity in small ruminants and resulting in substantial economic losses worldwide [1, 2]. This disease is widely distributed, with a high and often underestimated prevalence in dairy and meat-producing systems, including sheep (*Ovis aries*) flocks [3–5]. In small ruminants, the pathological spectrum ranges from focal intestinal lesions with minimal clinical impact to diffuse multibacillary enteritis associated with severe wasting and death [2, 6]. At the cellular level, Map shows a marked tropism for cells of the mononuclear phagocyte system; as intestinal and mesenteric macrophages, it constitutes the main niche for bacterial survival and replication and is central to granuloma formation and progression of lesions [7–10].

Control of paratuberculosis is challenging and relies on combinations of management, test-and-cull and vaccination [1, 11, 12]. In sheep, heat-inactivated whole-cell vaccines such as Gudair® are widely used as part of flock control programmes, particularly in countries with a high burden of ovine paratuberculosis such as Australia and New Zealand [11, 13]. Field and experimental studies have shown that vaccination reduces the incidence of clinical disease, faecal shedding and lesion severity and can prolong productive life [9, 13–15]. In parallel, several next-generation vaccine candidates, including live-attenuated, subunit, DNA and viral-vectored vaccines, are under experimental evaluation to improve protection and overcome the limitations of current vaccines [11, 16]. Because protection is greatest when animals are vaccinated before natural exposure to Map, vaccination is generally performed during the first weeks of life in endemic flocks [9, 11]. However, the early immunological mechanisms through which vaccination modulates and shapes host immune responses remain incompletely understood. Protection against Map has classically been linked to a Th1-dominated cellular immune response, with both IFN-γ-producing T cells and classically activated macrophages considered essential for mycobacterial control [2, 17]. Conversely, a shift towards a strong humoral response has often been associated with disease progression and multibacillary lesions. Nevertheless, this dichotomy has been challenged by recent work in sheep showing that antibodies may also contribute to protection at early stages [15, 17, 18].

Monocytes and macrophages are central to paratuberculosis because they serve as the primary cellular targets of Map and orchestrate many of the host's immune and pathological responses [2, 3]. In vitro studies have characterized the response of monocyte-derived macrophages (MDMs) against Map in murine and various ruminant models, including alterations in cellular metabolism [19], cytokine production [20], gene expression profiles [7] and overall functionality [8, 21]. Reactive oxygen species (ROS) generation and phagocytosis are core effector mechanisms of monocytes and macrophages [22, 23], commonly associated with IFN-γ-mediated activation and the acquisition of a phenotype capable of restricting Map growth [24]. Indeed, most inactivated vaccines developed against paratuberculosis for ruminants, including Gudair®, induce strong peripheral antigen-specific IFN-γ and other pro-inflammatory cytokine responses [15, 25]. However, none of these vaccines have demonstrated complete protection against Map. Moreover, recent studies in goat (*Capra hircus*) and cattle (*Bos taurus*) have shown that vaccination promotes granulomatous responses that are more effective at containing and eliminating Map following in vivo challenge [26] and can modulate early macrophage effector functions in vitro [20]. However, the number of studies characterizing the effects of vaccination on macrophages remains limited, especially in sheep, and important aspects of their functional behaviour have yet to be fully elucidated.

Beyond classical effector functions, accumulating evidence indicates that paratuberculosis vaccination may influence the functional state of innate immune cells through mechanisms associated with trained immunity, resulting in enhanced homologous and heterologous responsiveness, although the molecular mechanisms underlying these effects remain incompletely understood [27]. Such long-lasting changes in innate immune cell function may involve epigenetic mechanisms, including alterations in chromatin accessibility and histone modifications, as well as regulation by long non-coding RNAs (lncRNAs) [27, 28]. LncRNAs are > 200-nucleotide length RNA molecules, which do not code for proteins and participate in diverse regulatory processes at both the transcriptional and post-transcriptional levels [29]. These molecules have emerged as promising biomarkers for a wide range of diseases. In fact, several studies have described lncRNA alterations associated with paratuberculosis, both in tissues [30, 31] and in bovine MDMs [32–34]. Nevertheless, studies characterizing lncRNAs in the context of paratuberculosis vaccination are still limited, especially in sheep.

To gain a deeper insight into how paratuberculosis vaccination influences the functional responses of monocytes and MDMs, as well as associated lncRNA profiles, we performed a combined functional and transcriptomic analyses using an ovine model vaccinated with Gudair®.

Materials and methods

Animals

The experimental cohort consisted of ten male and female clinically healthy Assaf lambs of 15–20 days of age originating from the experimental flock of the Instituto de Ganadería de Montaña (CSIC-ULE; Grulleros, León, Spain). None of the animals had been previously vaccinated against paratuberculosis or showed clinical signs compatible with the disease and all lambs were confirmed seronegative for Map by indirect enzyme-linked immunosorbent assay (ELISA; ID Screen® Paratuberculosis Indirect, IDVet, Grabels, France). Lambs were randomly allocated into two groups: a vaccinated ($n = 5$) and a non-vaccinated control group ($n = 5$). Animals in the vaccinated group received a single 1 mL subcutaneous dose of the commercial Gudair® vaccine (CZ Vaccines, Porriño, Spain), formulated for small ruminants, administered in the brisket region.

Peripheral blood was sampled 1 day before vaccination (dpv) and at 30, 60 and 90 dpv (Figure 1). At each time point, 9 mL of whole blood were collected into BD Vacutainer™ tubes containing lithium heparin (Greiner Bio-One GmbH, Frickenhausen, Germany) for the IFN-γ release assay (IGRA) and for flow-cytometric assessment of phagocytic activity and ROS production. An additional, 9 mL of blood were obtained in tubes without anticoagulant (Greiner Bio-One GmbH, Frickenhausen, Germany) for the detection of Map-specific antibodies. At 90 dpv, 150 mL of heparinized blood was collected from each animal for the isolation of peripheral blood monocytes for lncRNA profiling and for the generation of OvMDMs for downstream functional assays (Figure 1).

Bacteria

Map K10 reference strain, plasmid-transformed Map K10 expressing tdTomato fluorescent protein (Map K10-tdTomato) and highly virulent bovine Map field isolate (strain 764) were used for in vitro functional assays. Map K10 and Map 764 strains were grown to exponential phase for approximately 3 weeks at 37 ± 1 °C in Middlebrook 7H9 broth supplemented with 10% oleic acid–albumin–dextrose–catalase (OADC; Becton Dickinson and Company, MD, USA), 0.2% glycerol, 0.05% Tween 80 (Panreac Química SA, Barcelona, Spain) and 2 mg/L mycobactin J (IDVET, Grabels, France) (7H9-OADC-MJ). In addition, Map K10-tdTomato was cultured under the same conditions with 25 µg/mL apramycin (7H9-OADC-MJ-apr) for plasmid maintenance. Map K10, Map K10-tdTomato and Map 764 suspensions were adjusted to 10^8 colony-forming units (CFU)/mL in a 1:1 glycerol:water solution. The inoculum concentration was estimated by optical density and subsequently confirmed by colony counting on solid agar medium. Aliquots of these suspensions were stored at −80 °C until required. Before each functional assay, frozen aliquots were thawed and resuspended in the appropriate fresh liquid culture medium for each strain (7H9-OADC-MJ for Map K10 and Map 764 and 7H9-OADC-MJ-apr for Map K10-tdTomato), followed by a 3-h incubation at 37 °C. Bacteria were then pelleted by centrifugation at 5000 × *g* for 10 min, washed twice with 1 × phosphate-buffered saline (PBS), and resuspended in RPMI 1640 medium with phenol red (Gibco®, Paisley, UK). To minimize bacterial clumping, suspensions were passed sequentially through 27- and 25-gauge needles and vortexed vigorously prior to use for in vitro infection. The Map 764 strain suspension was centrifuged

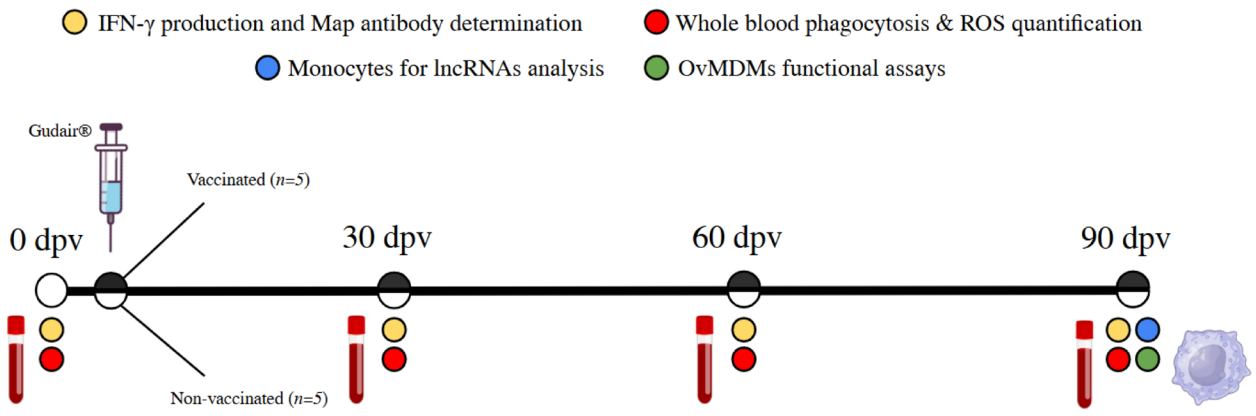

Figure 1 Experimental design overview. Lambs were divided into two groups: vaccinated with a heat-killed paratuberculosis vaccine Gudair® ($n = 5$) and non-vaccinated controls ($n = 5$). Blood samples were collected before vaccination and every 30 days up to 90 days post-vaccination (dpv) for analysis of specific interferon-gamma (IFN-γ) release and Map-specific antibodies (yellow dot) and phagocytic activity and ROS production (red dot). At 90 dpv, peripheral blood monocytes were isolated for both lncRNA profiling (blue dot) and differentiation into ovine monocyte-derived macrophages (OvMDMs) for functional assays (green dot).

at 10000 × *g* for 20 min and washed twice with 1X PBS. The resulting pellet was resuspended in 1X PBS and subjected to sonication on ice using a Vibra Cell 75186 sonicator (Thermo Fisher Scientific, Rochester, USA) in three 5 min cycles at 18 W. The protein content of the sonicate was determined using a NanoDrop® spectrophotometer (Thermo Fisher Scientific, Rochester, USA) and adjusted to a final concentration of 450 µg/mL.

Analysis of cell-mediated and humoral peripheral immune responses

Cell-mediated immunity was evaluated using an IFN-γ release assay. All samples were processed within 3 h after collection. Aliquots of whole blood were dispensed into 24-well tissue culture plates (Thermo Fisher Scientific, Rochester, USA) and stimulated with either 0.02 mg/mL avian purified protein derivative (PPDa; CZ Vaccines, Porriño, Spain), 0.02 mg/mL bovine purified protein derivative (PPDb; CZ Vaccines, Porriño, Spain), 450 µg/mL Map 764 strain sonicate (MS) or 1X PBS as an unstimulated negative control. After 22-h incubation at 37 °C, plates were centrifuged at 500 × *g* for 10 min, and plasma supernatants were collected and stored at −20 °C until analysis. IFN-γ release were determined in duplicate using a Bovigam® *Mycobacterium bovis* IFN-γ ELISA kit (Thermo Fisher Scientific, Rochester, USA), following manufacturer's recommendations. Absorbance was measured at 450 nm using an ELX800 microplate reader (Bio-Tek Instruments, Winooski, VT, USA). For each stimulus, normalized optical density (OD) values were used to calculate avian, bovine and MS index values, defined as the ratio between the mean OD of PPDa-, PPDb- or MS-stimulated samples and the mean OD of the corresponding negative control.

For humoral immune responses blood samples were allowed to clot for 24 h, after which serum was separated by centrifugation (500 g, 10 min), aliquoted and stored at −20 °C. Map-specific antibodies were quantified using the ID Screen® Paratuberculosis Indirect ELISA kit (Innovative Diagnostics, Montpellier, France) according to the manufacturer's instructions. Absorbance values were converted into sample-to-positive (S/P%) ratios by dividing the corrected OD of each sample by the corrected OD of the positive control and multiplying by 100.

Phagocytosis and ROS analysis in whole blood

ROS generation and phagocytic capacity of monocyte fraction in response to Map infection were assessed using flow cytometry using a sequential gating strategy [35]. ROS production was measured with the Respiratory Burst Assay Kit (Neutrophil/Monocyte) (Abcam Limited, Cambridge, UK), following the manufacturer's instructions. In brief, 100 µL of whole blood were dispensed into separate tubes and incubated with 0.05 mg of Dihydrorhodamine 123 (DHR 123) at 37 °C for 15 min to allow intracellular probe loading. Duplicate aliquots were subsequently stimulated with either 2.5 × 10^5 CFU of Map K10, 25 µL of 0.001 nM Phorbol-12-Myristate−13-Acetate (PMA) as a positive control or 1X PBS as a negative control to assess inducible ROS production. In parallel, phagocytic capacity was evaluated by incubating additional duplicate whole blood aliquots with 2.5 × 10^5 Map K10-tdTomato or 1X PBS as a negative control. Tubes for both assays were incubated for 30 min at 37 °C with 5% CO_2 in a humidified incubator. Following incubation, erythrocytes were lysed using the lysis buffer included in the kit, centrifugated and the remaining cells were resuspended in 200 µL of assay buffer for flow cytometric analysis.

Flow cytometry was carried out on a Cytek Aurora instrument (Cytek Biosciences, CA, USA). Monocyte fraction in whole blood was identified based on forward versus side scatter characteristics (FSC versus SSC), and doublets were excluded using FSC-A versus FSC-H (Additional file 1). Rhodamine 123 fluorescence, corresponding to the oxidized form of DHR 123, was measured at 508/529 nm (excitation/emission), whereas fluorescence from tdTomato-positive cells was detected at 554/579 nm. Thresholds were set using negative controls, and 10,000 events were recorded per sample. ROS production was expressed as the percentage and the mean fluorescence intensity (MFI) of Rhodamine 123-positive monocytes, while phagocytic capacity, defined as the combined binding and internalization of bacteria, was quantified as the percentage and the MFI of tdTomato-positive monocytes, indicating the relative bacterial load per cell.

Generation of ovine monocyte-derived macrophages (OvMDMs)

OvMDMs were generated from monocytes isolated from 150 mL of heparinized whole blood, as previously described [36]. Briefly, peripheral blood mononuclear cells (PBMCs) were separated by density gradient centrifugation using Lymphoprep™ (STEMCELL Technologies®, Cologne, Germany) and seeded into six-well plates (Thermo Fisher Scientific, Rochester, USA) for 3 h at 37 °C and 5% CO_2 in a humidified incubator. Non-adherent cells were removed by washing, and monocytes were cultured in RPMI 1640 medium supplemented with 10% foetal bovine serum (FBS) and 1% antibiotic–antimycotic solution (10000 units/mL of penicillin, 10 mg/mL of streptomycin and 25 µg/mL of amphotericin B) (Sigma-Aldrich, St. Louis, USA), and 60 ng/mL of ovine GM-CSF (KingFisher Biotech®, MN, USA). On day 7, OvMDMs were harvested using ice-cold

1X PBS containing 2 mM EDTA (PBS/EDTA) and gentle cell scraping. Then, OvMDMs were reseeded into 24-well culture plates (Thermo Fisher Scientific, Rochester, USA) at a density of 2×10^5 cells/well in antibiotic-free, supplemented RPMI 1640 and allowed to adhere for 24 h under the same culture conditions prior to the functional assays. Cell purity and viability were assessed by Trypan blue exclusion and flow cytometry, as previously described elsewhere [21].

Phagocytosis assay in OvMDMs

Phagocytosis capacity of OvMDMs against Map was assessed by flow cytometry, as previously described [20]. Briefly, 1×10^5 OvMDMs seeded in 24-well culture plates were stimulated in duplicate with Map-tdTomato at a MOI of 1:10 or with 1X PBS and incubated at 37 °C and 5% CO_2 for 3 h. After incubation, wells were washed twice with pre-warmed 1X PBS, and cells were detached using 10% trypsin–EDTA (Sigma-Aldrich, St. Louis, USA). Cells were subsequently harvested with 1 mL of ice-cold RPMI 1640 medium without antibiotic by gentle pipetting. Then, the OvMDMs were washed with 1X PBS containing 0.5% BSA and 2 mM EDTA (PBS/BSA/EDTA), fixed with 1% paraformaldehyde (Thermo Fisher Scientific, Rochester, USA) for 10 min at 4 °C and resuspended in PBS/EDTA/BSA for subsequent flow cytometry analysis.

Flow cytometry was performed using Cytek Aurora® flow cytometer (Cytek Biosciences, CA, USA), acquiring 10,000 events per sample. Phagocytosis capacity was quantified as both percentage of tdTomato-positive OvMDMs and MFI per sample, reflecting the combined binding and internalization of bacteria.

Bacterial killing assay in OvMDMs

The bactericidal activity of OvMDMs against Map was quantified by microbiological culture as previously described [37]. Briefly, 2×10^5 OvMDMs were seeded into 24-well culture plates by duplicate and infected with Map K10 at a MOI of 1:10, for 24 h at 37 °C and 5% CO_2. After incubation, supernatants were carefully collected, centrifuged to pellet non-internalized mycobacteria and wells were washed with 1X PBS to recover remaining non-internalized bacteria. The supernatant fraction was centrifuged, and the resulting pellet was resuspended in 1 mL of 1X PBS. Adherent cells in the well were lysed with 0.1% Triton X-100/PBS (Sigma-Aldrich, St. Louis, USA) for 10 min.

Serial ten-fold dilutions of both the supernatant and the lysate fractions were plated in duplicate onto Middlebrook 7H9-OADC-MJ. Then, plates were incubated at 37 °C for up to 2 months. CFUs were counted by direct plate counting, and the total number of viable CFU per sample was estimated. The remaining volumes of each fraction were stored at −20 °C for subsequent real-time polymerase chain reaction (qPCR)-based DNA quantification.

Bacterial DNA quantification in OvMDMs

Genomic DNA extraction of supernatant and cell lysate fractions from OvMDMs was performed using the DNeasy blood and tissue Qiagen kit (Qiagen Inc., Venlo, The Netherlands) following manufacturer instructions. DNA was quantified using Qubit 4 Fluorometer (Thermo Fisher Scientific, Rochester, USA).

Quantification of Map DNA was performed by real-time PCR (qPCR) using specific primers for Map *IS900* as previously described [20] employing a 7500 Real-Time PCR System (Applied Biosystems™, Spain). Reactions were carried out in triplicate with each 20 µL reaction mixture containing 0.5 µL of 250 nM of forward (MP10-1; [5′-ATG CGC CAC GAC TTG CAG CCT-3′]) and reverse (MP11-1; [5′-GGC ACG GCT CTT GTT GTA GTCG-3′]) Map primers, 10 µL of PowerUp™ SYBR™ Green Master Mix (Applied Biosystems*TM*, CA, USA) and 9 µL of template DNA. Thermocycling conditions included an initial activation at 95 °C for 10 min, followed by 40 cycles of 95 °C for 15 s and 60 °C for 1 min.

Standard curves were generated using ten-fold serial dilutions ranging from 1000 pg to 0.001 pg per reaction of genomic DNA extracted from 10^8 Map CFU. Samples were considered positive when the melting peak (Tm) was 89.1 ± 1.5 °C and threshold cycle (Ct) values were ≤ 37. The qPCR results were analysed using 7500 Software version 2.0.6 (Applied Biosystems™, Spain). Ct values were interpolated against the standard curve to estimate the amount of Map target DNA. This value was then converted into estimated Map bacterial equivalents by assuming 17 target copies per Map genome. For each sample, bacterial equivalents were calculated for each technical replicate, and the mean value was obtained from triplicate wells.

RNA extraction, library preparation and sequencing

Total RNA from 1×10^7 monocytes from each animal isolated at 90 dpv was extracted using the GeneMATRIX Universal RNA Purification Kit (GeneMATRIX Inc., Seongnam-si, South Korea) according to the manufacturer's instructions. Total RNA quantity and quality was determined by measuring absorbance with a NanoDrop (Thermo Fisher Scientific, Rochester, USA), and RNA integrity was assessed with an Agilent 5400 Bioanalyzer (Agilent Technologies, Santa Clara, CA, USA), yielding an RNA integrity number (RIN) of ≥ 7.7.

RNA library construction and sequencing were carried out at Novogene (Novogene Co., Ltd, Beijing, China).

Briefly, 500 ng of total RNA was used as input, and, after ribosomal RNA (rRNA) removal, double-stranded cDNA libraries were constructed using a NEBNext® Ultra™ Directional RNA Library Prep Kit (New England Biolabs, Ipswich, MA, USA) for Illumina, following the manufacturer's instructions. Sequencing was carried out on an Illumina NovaSeq X Plus sequencing platform (Illumina Inc., San Diego, CA, USA) using a 150 bp paired-end strategy. Library size distribution and quality were assessed using an Agilent 5400 Fragment Analyzer system (Agilent Technologies, Santa Clara, CA, USA). Raw sequencing data were deposited in the National Center for Biotechnology Information (NCBI) Sequence Read Archive (SRA) under BioProject accession number PRJNA1418281.

Bioinformatic analysis

Quality control of raw reads was carried out using Fastp (version 0.23.1), and Illumina adapters and low-quality reads (Phred score < 30) were removed using Bowtie2 (version 2.5.4). Clean reads were then mapped to the *Ovis aries* reference genome ARS-UI_Ramb_v3.0 using HISAT2 (version 2.2.1) and assigned to genes based on the Ensembl annotation. Transcriptome assembly was performed with StringTie (version 2.2.3) to identify novel lncRNA, which were subsequently merged with the reference annotation.

Candidate lncRNA transcripts were filtered by Pfamscan (version 1.6), and transcripts containing a known protein domain were excluded. In parallel, novel lncRNA candidates were predicted from the StringTie-assembled transcriptome. Transcripts shorter than 200 nucleotides or containing fewer than two exons were discarded, while those overlapping known protein-coding exons were excluded from the novel lncRNA candidate pool. Coding potential was assessed using Coding Potential Calculator 2 (CPC2; version 3.2.0) and Coding-Non-Coding Index (CNCI; version 2.0). Transcripts with CPC2 scores > 0 and CNCI scores > 0 were considered protein coding and excluded from the lncRNA set. Novel lncRNAs were then classified according to their genomic context following HUGO Gene Nomenclature Committee (HGNC) criteria [38] and merged with annotated lncRNAs to generate the final lncRNA catalogue. Finally, quantification of lncRNA was performed with StringTie (version 2.2.3) and normalized as fragments per kilobase of transcript per million mapped reads (FPKM).

In parallel, mRNA expression was quantified at the gene level using StringTie (version 2.2.3), generating FPKM values for the annotated protein-coding genes. Raw read counts were used as input for differential expression analysis with edgeR (version 4.0.16), with library-size normalization applied to account for differences in sequencing depth. Genes with an adjusted p-value (padj) ≤ 0.05 were considered differentially expressed. Results of the differential mRNA expression analysis are provided in Additional file 2.

Differential lncRNA expression analysis, target prediction and functional analysis

Expression levels of all lncRNAs were quantified, and differential expression between vaccinated and non-vaccinated animals was assessed using edgeR (version 4.0.16). Raw read counts were used as input for differential expression analysis and normalized for library size prior to statistical testing. LncRNA transcripts with FDR-adjusted p-values ≤ 0.05 and $\log_2$ fold change ≥ 2 were considered significantly differentially expressed (DE). Putative regulatory interactions were inferred using both cis and trans approaches. Cis-target genes were defined as protein-coding genes located within ± 100 kb of each lncRNA [39], whereas trans targets were identified based on significant expression correlations across samples [28].

Functional analysis of lncRNA was performed by evaluating Gene Ontology (GO) term and Kyoto Encyclopedia of Genes and Genomes (KEGG) pathway enrichment for predicted target genes of DE lncRNAs using clusterProfiler (version 4.8.1) [40], applying hypergeometric tests with Benjamini–Hochberg correction. Significantly enriched categories (adjusted p-values < 0.05) were used to infer the biological roles of vaccination-responsive lncRNAs, in line with current concepts of lncRNA-mediated gene regulation.

Statistical analysis

The normality of the data was checked using the Shapiro–Wilk test. Comparisons between vaccinated and non-vaccinated groups were performed using an unpaired Student's t-test. P-values < 0.05 were considered statistically significant. All statistical analyses were performed using GraphPad Prism version 8.0.1 (GraphPad Software, San Diego, California, USA).

Results

Cell-mediated and humoral peripheral immune response

A progressive increase in IFN-γ production was observed in the vaccinated group after stimulation with avian and bovine PPD and MS (Figure 2). From 60 dpv onward, IFN-γ index values in vaccinated lambs were significantly higher than in non-vaccinated controls in response to PPDb ($p < 0.01$; 2.02-fold increase) and MS ($p < 0.05$; 1.93-fold increase). Differences became more evident at 90 dpv, when responses to PPDa ($p < 0.01$; 9.06-fold increase), PPDb ($p < 0.001$; 2.75-fold increase) and MS ($p < 0.01$; 6.05-fold increase) were all significantly elevated

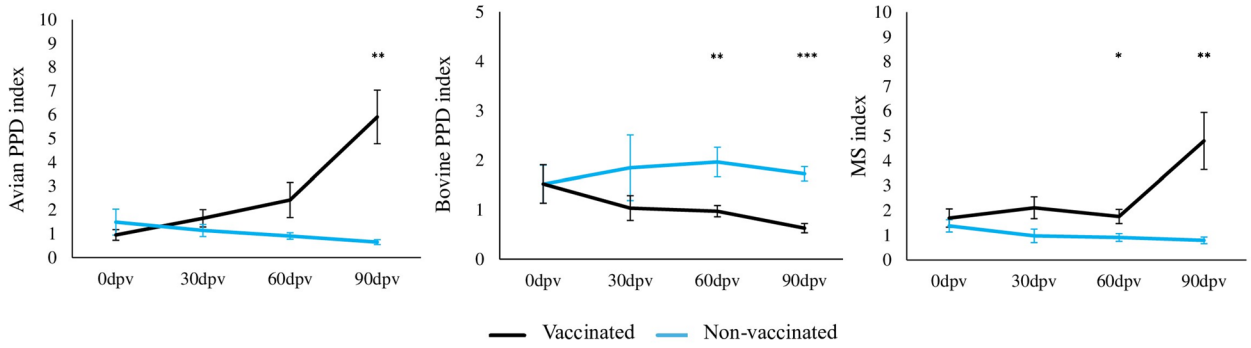

Figure 2 IFN-γ kinetics at different days post-vaccination (dpv). IFN-γ levels were measured following stimulation of whole blood with avian PPD, bovine PPD and Map 764 sonicate (MS) in animals vaccinated with Gudair® ($n = 5$) and non-vaccinated controls ($n = 5$). Index values were calculated by dividing the normalized absorbance of the antigen-stimulated samples by the normalized absorbance of control samples. Data were expressed as mean and standard error of the mean (SEM), and significant differences between vaccinated and non-vaccinated groups were represented as $^{*}p < 0.05$, $^{**}p < 0.01$ and $^{***}p < 0.001$.

in the vaccinated group. At this final time point, IFN-γ responses to avian PPD and MS were also 3.42-fold and 2.48-fold greater, respectively, than those elicited by bovine PPD in vaccinated animals ($p < 0.01$).

Map-specific antibodies were not detected in any of the non-vaccinated lambs at any time point (Figure 3). In contrast, vaccinated animals seroconverted rapidly, showing a marked rise in anti-Map antibody levels at 30 dpv ($p < 0.001$; 14.66-fold increase). Antibody titers remained significantly higher than in non-vaccinated at both 60 dpv ($p < 0.01$; 94.48-fold increase) and 90 dpv ($p < 0.001$; 117.35-fold increase).

Phagocytosis and ROS production in whole blood

Monocytes from the vaccinated group showed higher percentage of ROS production compared with the non-vaccinated group at 30, 60 and 90 dpv, corresponding to a 1.78-fold, 1.38-fold and 1.55-fold increase, respectively. However, statistical differences were observed only at 90 dpv ($p < 0.05$) (Table 1). No differences in the MFI were observed at any time point.

Regarding the percentage of tdTomato-positive monocytes, no statistically significant differences were found at any time point (Table 1). Similar to the ROS results, no differences in the MFI were observed at any time point.

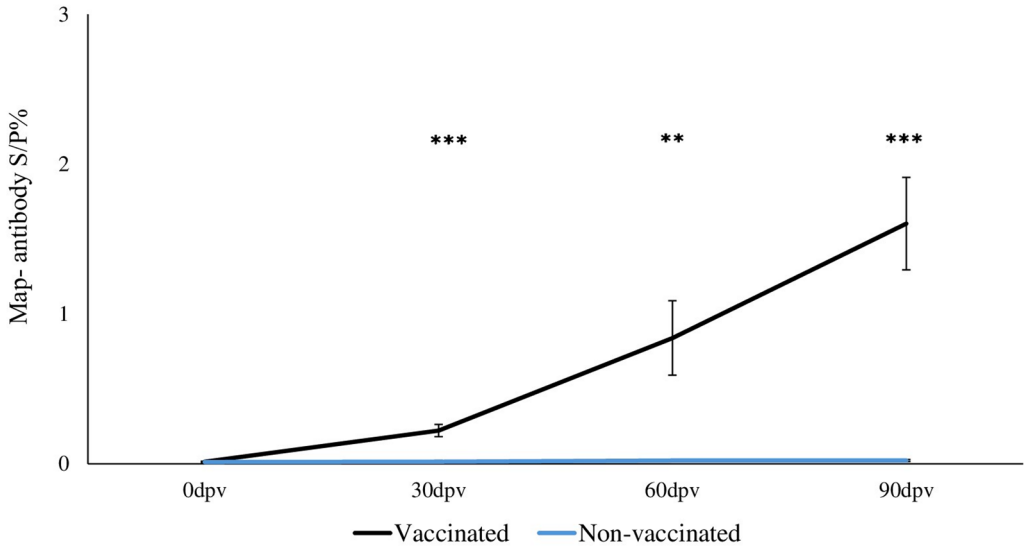

Figure 3 Map-specific antibody kinetics at different days post-vaccination (dpv). Values were expressed as a sample-to-positive (S/P%) ratio calculated by normalizing the difference between the sample and the negative control values to the difference between positive and negative control values. Data were expressed as mean and SEM (standard error of the mean) of animals vaccinated with Gudair® ($n = 5$) and non-vaccinated controls ($n = 5$). Significant differences between vaccinated and non-vaccinated groups were represented as $^{*}p < 0.05$, $^{**}p < 0.01$ and $^{***}p < 0.001$.

Table 1 tdTomato$^+$ monocytes and ROS production after in vitro Map infection of whole blood

Groups	Dpv	Percentage (%) tdTomato$^+$	MFI tdTomato$^+$	Percentage (%) ROS	ROS MFI
Vaccinated	30	7.73 ± 0.41	7505 ± 994	1.88 ± 0.45	4265 ± 993
	60	6.05 ± 0.76	5913 ± 803	2.11 ± 0.34	2695 ± 255
	90	5.99 ± 0.48	6181 ± 479	3.69 ± 0.36*	3036 ± 390
Non-vaccinated	30	5.64 ± 0.67	5542 ± 767	1.06 ± 0.11	3839 ± 362
	60	8.92 ± 0.89	9025 ± 1046	1.53 ± 0.21	2580 ± 417
	90	5.34 ± 0.45	4262 ± 378	2.37 ± 0.31*	2306 ± 127

Percentage (%) and mean fluorescence intensity (MFI) were assessed in vaccinated ($n = 5$) and non-vaccinated animals ($n = 5$) at 30, 60 and 90 days after vaccination (dpv). Monocytes were selected by flow cytometry based on their morphology, using forward (FSC) and side scatter (SSC) parameters. Data are expressed as mean values and SEM (standard error of the mean), and significant differences between vaccinated and non-vaccinated groups were represented as $^*p < 0.05$.

Phagocytosis in OvMDMs

Phagocytic activity against Map was also assessed in OvMDMs generated at 90 dpv. No significant differences were found between vaccinated and non-vaccinated groups, either in the percentage of tdTomato-positive cells (59.83% and 58.40%, respectively) or in MFI (125,867 and 129,921, respectively) (Figure 4).

Bacterial killing in OvMDMs

Map viability was assessed in both the supernatants and cell lysates of OvMDMs using microbiological culture. Higher numbers of viable Map were detected in supernatants than in cell lysates (1.88-fold increase), although this difference did not reach statistical significance (Figure 5). Within each fraction, CFU counts from vaccinated animals were slightly higher than those from non-vaccinated animals (1.13-fold in supernatants and 1.44-fold in lysates), but these differences were not statistically significant either.

Bacterial DNA quantification in OvMDMs

Map DNA was quantified in supernatants and cell lysates from OvMDMs and expressed as estimated Map bacterial equivalents using the standard curve (Figure 6). Overall, vaccinated animals tended to show increased Map bacterial equivalents compared with non-vaccinated animals, with a 2.40-fold increase in supernatants and a 1.76-fold increase in cell lysates. However, none of these differences reached statistical significance.

Quality filtering, mapping and assembly

Quality control of the ten monocytes samples using fastp indicated consistently high sequencing quality (Additional file 3). On average, 84.96 million raw reads

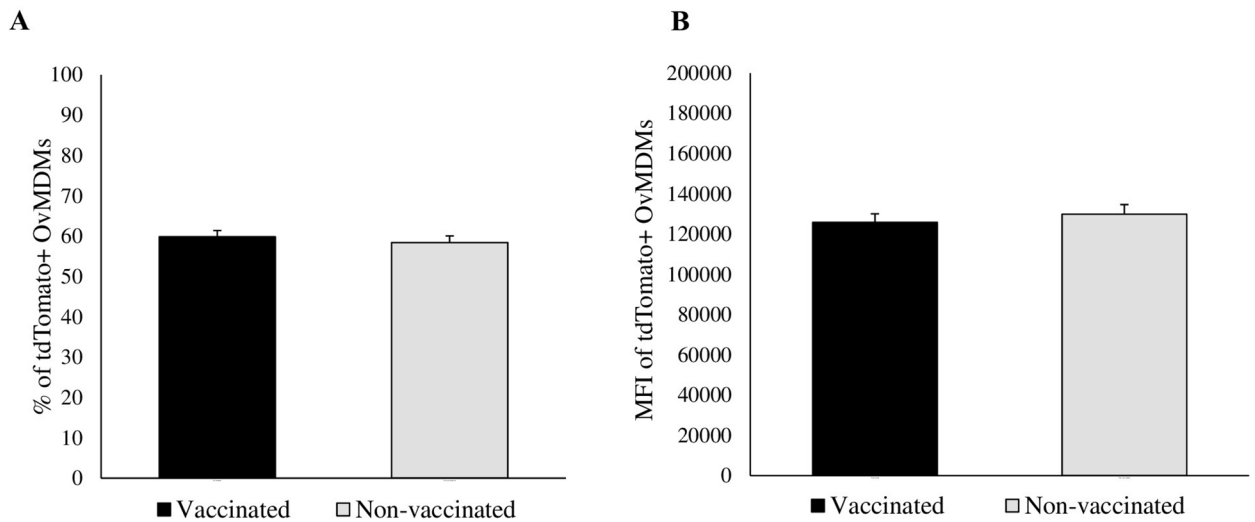

Figure 4 Phagocytic activity of OvMDMs generated from peripheral blood. Phagocytosis of vaccinated and non-vaccinated animals at 90 days post-vaccination (dpv) in response to in vitro infection with *Mycobacterium avium* subsp. *paratuberculosis* (Map). Phagocytosis (binding + internalization) was assessed as the percentage of tdTomato + OvMDMs **(A)** and mean fluorescence intensity (MFI) **(B)**. Data are expressed as mean values and SEM (standard error of the mean).

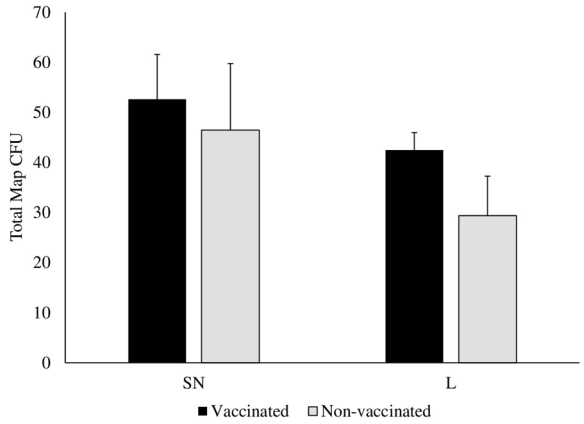

Figure 5 Total viable Map counts in OvMDMs generated from vaccinated and non-vaccinated animals at 90 days post-vaccination. Data are expressed as mean values and SEM (standard error of the mean) of CFU counts from both supernatant (SN) and lysed cells (L) fractions.

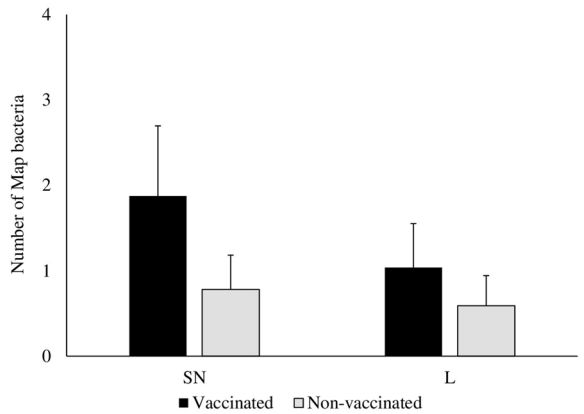

Figure 6 Map equivalent bacterial load in OvMDMs generated from vaccinated and non-vaccinated groups. Quantification of *IS900* sequence was performed by real-time qPCR in supernatants (SN) and lysed cells (L) fractions. Data are expressed as mean values and SEM (standard error of the mean).

were obtained, with 97.8% retained after filtering. The mean Q20 and Q30 scores were 98.78% and 95.93%, respectively, and the average GC content was 50.89%. Pre-processed reads were mapped against the reference genome (ARS-UI_Ramb_v3.0) with a mean mapping rate of 95.16%. Most reads aligned uniquely (88.05%), while a smaller fraction was multi-mapped (7.11%), and 84.81% of reads were properly paired indicating robust alignment. Mapped reads were primarily located in exonic regions (69.50%), with smaller fractions mapping to intergenic (18.65%) and intronic regions (11.85%).

lncRNA identification

Following the sequential filtering strategy, 6854 lncRNA transcripts were consistently identified in monocytes including 2135 novel and 4719 annotated transcripts. Chromosome 1 and chromosome 3 harboured the largest fractions of lncRNAs (8.91% and 8.613%, respectively), followed by chromosome 2 (7.03%). According to the mutually exclusive genomic classification used in the bioinformatic pipeline, most novel lncRNAs were classified as intergenic (59.11%), followed by intronic lncRNAs (14.85%) and antisense (8.15%), whereas the remaining 17.89% were assigned to other genomic categories.

Differential expression of lncRNA

Differential expression analysis was conducted for lncRNAs by comparing monocytes from vaccinated versus non-vaccinated animals. A total of four lncRNAs transcripts were found differentially expressed (DE), of which three corresponded to novel lncRNAs and one to previously annotated lncRNAs. Among these transcripts, three were upregulated and one downregulated ($padj \leq 0.05$, $|\log_2 FoldChange| \geq 2$) (Table 2). Three DE lncRNAs, TCONS_00049372, TCONS_00049376 and TCONS_00049380, arose from the same genomic locus (XLOC_015839) on chromosome 7 and were consistent with distinct transcript isoforms, while the remaining DE lncRNA was located in chromosome 2.

Cis-target assignment and trans co-expression analysis of DE lncRNAs

At least one proximal protein coding gene within ± 100 kb was found in all DE lncRNAs, as summarized in Table 3. Three DE lncRNAs were close to the nuclear export mediator factor (*nemf*), kelch domain containing

Table 2 Differentially expressed lncRNAs in isolated monocytes from vaccinated versus non-vaccinated lambs

Transcript ID	Category	Chromosome	$Log_2FoldChange$	*padj*
TCONS_00049372	Novel	7	16.57	0.000369
TCONS_00049376	Novel	7	17.63	0.004388
TCONS_00049380	Novel	7	17.51	0.006494
TCONS_00018201	Annotated	2	−12.19	0.0310389

Category indicates whether the transcript was previously annotated or assembled as novel. $Log_2FoldChange$ is expressed as vaccinated relative to non-vaccinated (positive values indicate upregulation in vaccinated lambs).

Table 3 Prediction of target genes for DE lncRNA cis regulation

LncRNA transcript	Chromosome	Gene name
TCONS_00018201	2	*palld, cbr4*
TCONS_00049372	7	*Nemf, klhdc1, klhdc2, arf6*
TCONS_00049376	7	*Nemf, klhdc1, klhdc2, arf6*
TCONS_00049380	7	*Nemf, klhdc1, klhdc2, arf6*

DE lncRNAs from vaccinated versus non-vaccinated groups are listed with their chromosome location and nearby protein-coding potentially regulated in cis.

Table 4 Prediction of trans co-expressed target genes for DE lncRNAs

Transcript_id	Number of genes	Gene name
TCONS_00049376	10	*rtn1, hpx, anhx, cripto, elapor1, flt, or4f3, or1e2, or52j3, or51g1*
TCONS_00049372	3	*gstcd, ccdc116, y lage3*

For each DE lncRNA, the number of significantly co-expressed protein-coding genes is shown. All pairs meet a Pearson correlation > 0.95 and a *p*-value < 10^{-6}

1 (*klhdc1*), ADP-ribosylation factor 6 (*arf6*) and kelch domain containing 12 (*klhdc2*) genes, while the remaining lncRNA was close to palladin, cytoskeletal-associated protein gene (*palld*) and the carbonyl reductase 4 gene (*cbr4*), and all these genes significantly enriched the GO term 'ubiquitin-dependent protein catabolic process via the C-end degron rule pathway'. In terms of trans interactions, only two of the four DE lncRNA showed robust co-expression with protein-coding genes (Table 4). In more detail, the most DE lncRNA, TCONS_00049376, was correlated with 10 genes which significantly enriched the KEGG pathway 'olfactory transduction' (*p*-values = 1.19E−9), while TCONS_00049372 was associated with GSTCD, CCDC116 and y LAGE3.

None of the genes identified as potential cis or trans targets of the DE lncRNA were differentially expressed at the mRNA level (Additional file 2).

Discussion

Paratuberculosis control strategies remain a challenging endeavour because currently commercially available vaccines primarily mitigate disease severity and bacterial shedding rather than preventing infection, and the mechanisms underlying protective immunity remain incompletely understood [2, 11]. This limitation is particularly relevant given the complex interplay between cellular and humoral responses, especially in tissue-level control, which primarily depends on macrophage functional states that govern bacterial clearance and shape the local inflammatory milieu [15, 41]. In this context, in vitro and ex vivo approaches using cultured MDMs provide controlled platforms to elucidate how vaccination reshapes innate effector functions [8, 20]. Thus, the present study analysed monocyte and OvMDMs functional responses after paratuberculosis vaccination in an ovine model. Vaccination enhanced monocyte oxidative burst in whole blood; in contrast, the microbicidal activity of OvMDMs differentiated in vitro showed only limited changes. In parallel, transcriptomic analysis of isolated blood monocytes identified a high number of novel lncRNAs. In addition, among the lncRNA identified, four were differentially expressed in vaccinated animals, indicating a modest reshaping of monocyte expression patterns, which may reflect changes in monocyte functional responses.

In the present study, vaccinated lambs displayed an early and sustained antigen-specific IFN-γ response, together with a progressive rise in Map-specific antibody levels, demonstrating that vaccination induces sustained modulation of peripheral immune responses. This finding is consistent with previous works in sheep where Gudair® vaccination generated a specific peripheral immune response characterized by high levels of IFN-γ and Map-specific antibodies that start 2–3 weeks after vaccination and can remain detectable for at least 12 months post-vaccination [15, 42]. IFN-γ production has been widely associated with protective cell-mediated immune responses and control of Map infection [1, 2]. Monocytes and macrophages respond to IFN-γ stimulation by upregulating antimicrobial effector pathways, including inducible nitric oxide synthase (iNOS) expression and phagolysosome maturation [21, 25]. The production of ROS is one of the antimicrobial mechanisms triggered following Map uptake, contributing to intracellular mycobacterial killing [21], and was significantly enhanced in monocytes from vaccinated animals. This process is largely dependent on pro-inflammatory cytokines that activate monocytes to produce large amounts of superoxide anion (O_2^-) that promote the elimination of phagocytosed mycobacteria [43]. Cytokines such as IFN-γ, TNF-α and GM-CSF have been directly linked to an amplified oxidative burst in human and bovine macrophages [44–46]. Therefore, this augmented oxidative response observed in our study likely reflects the elevated production of pro-inflammatory cytokines such as IFN-γ by lymphocytes and other immune cells present in whole blood of vaccinated animals [24, 47]. By contrast, high serum anti-Map IgG levels have traditionally been considered a hallmark of advanced disease and active bacterial shedding [48]. However, evidence from vaccine studies suggest that an early vaccine-induced antibody response can be compatible with protection, likely by promoting opsonization prior macrophage phagocytosis

[15, 49]. In our study, no differences were found in phagocytic capacity between monocytes from vaccinated and non-vaccinated lambs. One possible explanation is that Map could have been more rapidly degraded after uptake because of the higher ROS production observed in vaccinated monocytes. In addition, circulating monocytes are smaller and less differentiated precursors compared with fully mature tissue macrophages [50] and may have a relatively limited phagocytic capacity. This intrinsic limitation could contribute to the lack of measurable differences in phagocytosis, despite potentially enhanced intracellular microbicidal activity in vaccinated animals.

Monocyte-to-macrophage differentiation is accompanied by functional maturation, consistent with the specialized phagocytic role of macrophages, as some studies have assessed [51, 52]. OvMDMs from vaccinated animals consistently showed higher Map loads, as determined by both culture and qPCR, although these differences did not reach statistical significance, likely due to the variability among animals. This observation may suggest a trend towards increased bacterial uptake in macrophage from vaccinated animals. Similar increased phagocytosis of Map has been reported in caprine MDMs from vaccinated animals with Silirum®, although, in that study, phagocytosis was assessed at 30 days post-vaccination by immunofluorescence, rather than at 90 dpv [20]. Thus, despite methodological and species-related differences among studies, Map vaccination may influence the phagocytic capacity of MDMs, although these effects may not be fully captured at the post-vaccination time point evaluated in the present study. Additional studies at different post-vaccination time points are therefore needed to determine the magnitude, persistence and temporal dynamics of these macrophage responses. Another plausible explanation for the limited differences observed in isolated OvMDMs is that optimal macrophage activation may require coordinated interactions with other leukocyte populations and humoral factors, which are absent under isolated culture conditions. Consistent with this hypothesis, enhanced phagocytosis of Bacillus Calmette–Guérin (BCG) and Map was observed in human MDMs cultured with autologous serum containing vaccine-induced IgG antibodies while a 1:1 co-culture of bovine neutrophils and macrophages exposed to Map displayed greater phagocytic activity than either cell population alone, supporting a synergistic interaction [35]. Therefore, protective immunity may also rely on coordinated interactions among multiple immune cell populations and antibodies than on macrophage-intrinsic microbicidal activity alone [53].

Since the functional phenotype of innate immune cells is largely dictated by their underlying transcriptional programmes, epigenetic regulation is increasingly recognized as a key layer of control in mycobacterial infections, including paratuberculosis [29, 54]. Within this framework, lncRNAs are particularly relevant because they can tune gene expression and have been implicated in modulating the magnitude and durability of antimicrobial responses [55]. Studies on tuberculosis and paratuberculosis have identified Map-responsive lncRNAs linked to immune pathways in bovine macrophages, supporting their potential involvement in the regulation of antimicrobial immunity [31–33, 56]. In this study, we provide a robust ovine dataset and identified 6854 monocyte lncRNAs, of which 2135 were novel. Other studies employing bovine MDMs infected with Map discovered 13,301 (605 novel) lncRNAs [32] or 397 novel lncRNAs [31], which aligns with our dataset. The fact that 31.15% of the detected lncRNAs were novel indicates that lncRNAs remain under-annotated, highlighting the limited transcriptomic characterization of the sheep model relative to more extensively curated reference species [29, 32].

Interestingly, the identified lncRNAs were not evenly distributed across the ovine genome, with most transcripts mapping to chromosomes 1, 2, 3 and 7. Although chromosomal localization alone does not imply functional relevance, these chromosomes contain genomic regions previously associated with immune-related processes in ovine PBMCs, including in cytokine production and monocyte markers [57]. This distribution suggests that the identified lncRNAs may preferentially arise from genomic regions involved in immune regulation, although functional studies will be required to determine whether they contribute to the immune response against Map. In this study we identified four DE lncRNAs transcripts between vaccinated and non-vaccinated monocytes, including three novel transcripts and one previously annotated. Notably, three of the four DE lncRNAs transcripts corresponded to alternative isoforms arising from a single genomic locus on chromosome 7 rather than independent lncRNA loci. Given that these isoforms were identified computationally, their biological significance should be interpreted cautiously and requires experimental validation. The clustering of these transcripts within the same genomic locus is consistent with bovine paratuberculosis studies reporting a high proportion of novel lncRNAs and DE lncRNAs on this chromosome, although the functional significance of the clustering observed in this study remains unclear [31, 34]. Most lncRNA studies in paratuberculosis have focused on disease stage or Map infection signatures, with no studies to date addressing lncRNA profiles associated with vaccination against paratuberculosis. Higher numbers of DE lncRNAs have been reported in bovine macrophages following Map infection, indicating

that infection elicits a broader lncRNA transcriptional response than vaccination alone [29–33]. Some of these studies identified Map-responsive lncRNAs in infected bovine MDMs and linked them to core innate inflammatory programmes, such as NF-κB routes, chemokine (IL-8) signalling and TLR–MyD88 pathways [31–33, 58]. Likewise, analyses of intestinal tissues from cattle at different stages of paratuberculosis have identified lncRNA signatures linked to mucosal immune functions, including antigen presentation and host-defence mechanisms [29, 30]. Together, these findings suggest that vaccination induces a comparatively subtle modulation of the lncRNA landscape in circulating monocytes. The observed chromosomal distribution highlights specific genomic regions in which vaccine-associated lncRNAs were identified; however, whether this distribution has functional significance remains to be determined.

LncRNAs can regulate gene expression either locally through genomic co-localization to proximal genes (cis) or by co-expression with functionally distant linked genes (trans). Therefore, predicting cis- and trans-associated targets can provide a basis for functional enrichment analysis to identify pathways potentially associated with DE lncRNAs. Regarding co-localization, several of the top DE lncRNAs in vaccinated animals were located near genes involved in macrophage activation and inflammatory signalling. Three upregulated lncRNAs (TCONS_00049372, TCONS_00049376 and TCONS_00049380) mapped close to *arf6*, *nemf*, *klhdc1* and *klhdc2*. Among these, *arf6* is particularly relevant because it regulates membrane trafficking, actin remodelling and phagosome formation [59] – processes that are critical for macrophage interaction with intracellular pathogens and are known targets of Map survival strategies [60, 61]. Although phagocytosis and intracellular bacterial survival were not significantly altered in the present study, the trend towards increased Map recovery in macrophages from vaccinated animals and the proximity of these candidate lncRNAs to genes involved in vesicular trafficking and phagosome formation may point to a potential link with these pathways following vaccination. In contrast, *nemf*, *klhdc1* and *klhdc2* participate in complementary protein quality-control pathways, and specifically *nemf* has been identified as DE gene in the blood of tuberculosis-infected individuals [62–64]. Consistently, GO enrichment analysis of the genes co-localized with these DE lncRNAs identified the significantly enriched biological process 'ubiquitin-dependent protein catabolic process via the C-end degron rule pathway', suggesting a potential association with protein quality control involved in phagocyte activation and homeostasis. Conversely, the downregulated lncRNA PALLD-IT5 (TCONS_00018201) was located near *palld* and *cbr4*. *palld* encodes palladin, a protein involved in the organization of actin filaments which is essential for phagocytic cup formation and engulfment [65, 66]. Notably, *palld* was among the differentially expressed genes in peripheral blood during a murine *Mycobacterium tuberculosis* infection [67], further supporting its involvement in host response to mycobacterial challenge. Therefore, changes in the expression of this lncRNA may be associated with genes involved in cytoskeletal dynamics in monocytes following vaccination. Moreover, *cbr4* is involved in fatty-acid and lipid metabolism and was also identified within a miRNA–mRNA regulatory network in jejunal lymph nodes from Map-infected cattle [68, 69]. Lipid metabolic pathways are increasingly recognized as key regulators of monocyte and macrophage activation, which is particularly relevant to Map, as this pathogen can manipulate host lipid metabolism, promote the formation of cholesterol-rich intracellular compartments within macrophages and persist within these niches [18]. Although the functional significance of *cbr4* modulation remains to be established, its proximity to PALLD-IT5 raises the possibility that this lncRNA may be associated with metabolic pathways of monocytes following vaccination, potentially supporting their activation and functional response during Map infection.

Trans co-expression analysis suggested that TCONS_00049372 and TCONS_00049376 were associated with genes involved in diverse cellular processes. Among these, *hpx* and *ftl* are key regulators of oxidative stress and iron homeostasis, respectively, both of which are central to host responses during mycobacterial infection [70, 71]. In fact, *hpx* has been reported to be upregulated in mesenteric lymph nodes from Map-infected mice, while *ftl* is also induced in granulocytes of BCG-vaccinated guinea pigs, supporting the relevance of iron sequestration and oxidative stress regulation in host–mycobacteria interactions [69, 70]. These associations raise the possibility that the identified lncRNAs may be linked to pathways related to oxidative stress and iron homeostasis following vaccination, although this interpretation requires functional validation. Besides, *elapor1*, also known as *kiaa1324*, encodes a transmembrane protein involved in autophagy and the regulation of cell survival [72]. Consistently, the related gene *kiaa1324l* was downregulated in blood and ileocecal tissue from naturally Map-infected cattle [73], further suggesting an association between this gene family and host–pathogen interactions during paratuberculosis. Finally, TCONS_00049376 was co-expressed with four predicted loci (LOC101119825, LOC101109894, LOC101107990 and LOC101108773), annotated based on similarity to human olfactory receptor genes *or4f3*, *or1e2*, *or52j3* and *or51g1*, respectively. Although

olfactory receptor genes were originally considered to be restricted to the olfactory epithelium, transcriptomic studies in cattle have identified their expression in a wide range of non-olfactory tissues, suggesting that some member of this family may have functions beyond odour perception [74]. Indeed, olfactory receptors belong to the G protein-coupled receptor (GPCR) superfamily, and growing evidence indicates that ectopically expressed receptors regulate diverse physiological processes, including calcium signalling, cell migration, proliferation and immune responses [75, 76]. In mouse vascular macrophages, specific olfactory receptors have been shown to act as chemosensors, triggering NLRP3 inflammasome activation, IL-1β secretion and ROS production [77]. Moreover, GPCR-mediated signalling has emerged as an important mechanism linking microbial metabolites with intestinal immune homeostasis and chronic inflammatory disorders [78]. However, because olfactory receptors constitute the largest multigene family in mammals, enrichment analyses may reflect annotation bias and should therefore be interpreted with caution and their potential role in vaccine-induced responses requires further investigation. Importantly, the genes identified as potential targets of the DE lncRNAs did not show corresponding changes in mRNA expression. It is possible that vaccination alone was not sufficient to induce a strong transcriptional response at the mRNA level, whereas changes in lncRNA expression may be detectable and could reflect early regulatory responses to vaccination. Additional stimuli, such as pathogen challenge, may elicit more pronounced transcriptional changes. Therefore, these predicted lncRNA–gene relationships should be considered potential regulatory associations requiring further investigation.

In conclusion, this work expands current knowledge of ovine lncRNAs, revealing a large fraction of novel transcripts and, to our knowledge, providing the first description of paratuberculosis vaccination-associated lncRNA modulation in sheep monocytes. Functionally, vaccination was associated with a higher proportion of ROS-positive circulating monocytes, whereas OvMDMs at 90 dpv did not show significant differences, although phagocytosis was increased 24 h after infection. Although these functional changes were modest, transcriptomic profiling of infected OvMDMs may reveal vaccine-associated molecular signatures in these cells, providing further insight into the molecular response associated with vaccination. Overall, our findings provide a foundation for further studies investigating the functional relevance of vaccine-associated lncRNA and their potential involvement in the innate immune response and protection against Map infection.

Supplementary information

The online version contains supplementary material available at https://doi.org/10.1186/s13567-026-01878-9.

Additional file 1. Gating strategy of whole blood monocyte phagocytosis and ROS production by flow cytometry. In the first step, leukocytes were identified based on forward scatter (FSC-A) and side scatter (SSC-A) properties. In the second step, a doublet discrimination strategy was applied using FSC-A versus FSC-H to exclude cell aggregates. For the phagocytosis assay (A), tdTomato positive monocytes were identified in the Yellowgreen-1 channel and considered positive for Map uptake. For the ROS assay (B), 123-DHR positive monocytes were identified based on fluorescence intensity in the Blue-3 channel. Uninfected controls were used to adjust scatter-based gates and fluorescence thresholds. Flow cytometry data from 10,000 monocytes per animal were acquired and analysed using Cytek Aurora® flow cytometer (Cytek Biosciences, CA, USA).

Additional file 2. Differential mRNA expression analysis of isolated monocytes from vaccinated versus non-vaccinated lambs at 90 days post-vaccination. The table contains gene identifiers, descriptions and loci; individual FPKM values, mean expression values for each group, $\log_2$ fold changes, *p*-values and Benjamini-Hochberg-adjusted *p*-values (padj).

Additional file 3. fastp quality-control summary for monocyte RNA-seq libraries. fastp quality-control metrics for each monocyte RNA-seq library, including raw and clean read counts and bases after filtering, estimated sequencing error rate, the percentage of bases with Phred quality scores ≥ Q30, and GC content (%), total clean reads, the overall mapping rate to the reference genome (ARS-UI_Ramb_v3.0), and the percentages of uniquely and multi-mapped reads.

Acknowledgements
We would like to thank the staff of Instituto de Ganadería de Montaña (CSIC-ULE) for the handling and sampling of experimental animals.

Authors' contributions
Conceptualization: M.F. Methodology: M.F., J.B.S., P.M.G., N.A.V., M.M.U., N.E., M.C., M.S., E.M. and I.F. Investigation: P.M.G. and N.A.V. Data curation: P.M.G. and N.A.V. Formal analysis: P.M.G., N.A.V. and I.F. Resources: M.F., N.E., J.B. and D.G.E. Writing – original draft: P.M.G. Writing – review and editing: all authors. Supervision: M.F.

Funding
This study was funded by Ministerio de Ciencia e Innovación (Agencia Estatal de Investigación; AEI) co-funded with the European Union, project reference PID2021-125807OB-C21 (PARAINVAX). P.M.G. was supported by a Junta de Castilla y León predoctoral contract (Orden EDU/1868/2022), co-funded by ESF+. M.S. was hired with the funding of this project. N.A.V. was the recipient of a postdoctoral contract (LE058P23) from the Junta de Castilla y León. M.M. was the recipient of a predoctoral grant from the Department of Science, Universities and Innovation of the Basque Government.

Data availability
RNA-seq raw sequencing data of this study have been deposited in the National Center for Biotechnology Information (NCBI) Sequence Read Archive (SRA) under BioProject (PRJNA1418281) or through the following link: https://www.ncbi.nlm.nih.gov/bioproject/?term=PRJNA1418281. Additional data supporting the findings of this study are available from the corresponding author upon reasonable request.

Declarations

Ethics approval and consent to participate
All animal procedures were carried out in accordance with current European and Spanish regulations on the use of animals for scientific purposes. The study protocol was reviewed and approved by the bioethics committee of the Instituto de Ganadería de Montaña (CSIC-ULE) (IGM 100102/2025–03); the handling of lambs and collection of blood samples was assured to not cause pain, suffering or distress.

Consent for publication
Not applicable.

Competing interests
The authors declare no competing interests.

Author details
[1]Grupo de Investigación en Sanidad y Patología de Rumiantes (SANPATRUM), Universidad de León, Campus de Vegazana s/n, 24071 León, Spain. [2]Instituto de Ganadería de Montaña (IGM), (CSIC–Universidad de León), Grulleros, León, Spain. [3]Animal Science Department, NEIKER-Basque Institute for Agricultural Research and Development Basque Research and Technology Alliance (BRTA), Derio, Bizkaia, Spain.

Received: 17 April 2026 Accepted: 26 October 2026
Published online: 18 November 2026

References

1. Whittington R, Donat K, Weber MF, Kelton D, Nielsen SS, Eisenberg S, Arrigoni N, Juste R, Sáez JL, Dhand N, Santi A, Michel A, Barkema H, Kralik P, Kostoulas P, Citer L, Griffin F, Barwell R, Moreira MAS, Slana I, Koehler H, Singh SV, Yoo HS, Chávez-Gris G, Goodridge A, Ocepek M, Garrido J, Stevenson K, Collins M, Alonso B et al (2019) Control of paratuberculosis: who, why and how. A review of 48 countries. BMC Vet Res 15:198
2. Sweeney RW (2011) Pathogenesis of paratuberculosis. Vet Clin North Am Food Anim Pract 27:537–546
3. Windsor PA (2015) Paratuberculosis in sheep and goats. Vet Microbiol 181:161–169
4. Idris SM, Eltom KH, Okuni JB, Ojok L, Elmagzoub WA, El Wahed AA, Eltayeb E, Gameel AA (2022) Paratuberculosis: the hidden killer of small ruminants. Animals (Basel) 12:12
5. Magalhães NMAdeA, Limeira CH, Costa RDL, Portela RA, Azevedo SS, Alves FSF, Alves CJ (2025) Global prevalence of *Mycobacterium avium* subsp. *paratuberculosis* in sheep: systematic review and meta-analysis. Small Rumin Res 243:107430
6. Pérez V, García Marín JF, Badiola JJ (1996) Description and classification of different types of lesion associated with natural paratuberculosis infection in sheep. J Comp Pathol 114:107–122
7. Weiss DJ, Evanson OA, Deng M, Abrahamsen MS (2004) Gene expression and antimicrobial activity of bovine macrophages in response to *Mycobacterium avium* subsp. *paratuberculosis*. Vet Pathol 41:326–337
8. Mitchell RM, Gollnick NS, Sreevatsan S, Russell DG, Schukken YH (2011) Quantification of *Mycobacterium avium* subsp. *paratuberculosis* (MAP) survival in monocyte-derived macrophages. Vet Immunol Immunopathol 139:73–78
9. Fernández M, Royo M, Fuertes M, Arteche-Villasol N, Ferreras MC, Benavides J, Pérez V (2022) Effects of paratuberculosis vaccination at different ages in a dairy goat herd: a 2-year follow-up. Animals (Basel) 12:3135
10. Zapico D, Espinosa J, Criado M, Gutiérrez D, Ferreras MC, Benavides J, Pérez V, Fernández M (2025) Immunohistochemical expression of TLR1, TLR2, TLR4, and TLR9 in the different types of lesions associated with bovine paratuberculosis. Vet Pathol 62:305–318
11. Bastida F, Juste RA (2011) Paratuberculosis control: a review with a focus on vaccination. J Immune Based Ther Vaccines 9:8
12. Juste RA, Perez V (2011) Control of paratuberculosis in sheep and goats. Vet Clin North Am Food Anim Pract 27:127–138
13. Juste RA, Geijo MV, Elguezabal N, Sevilla IA, Alonso-Hearn M, Garrido JM (2021) Paratuberculosis vaccination specific and non-specific effects on cattle lifespan. Vaccine 39:1631–1641
14. Windsor PA (2013) Understanding the efficacy of vaccination in controlling ovine paratuberculosis. Small Rumin Res 110:161–164
15. Pooley HB, Begg DJ, Plain KM, Whittington RJ, Purdie AC, de Silva K (2019) The humoral immune response is essential for successful vaccine protection against paratuberculosis in sheep. BMC Vet Res 15:223
16. Mahmoud AH, Abdellrazeq GS, Franceschi V, Schneider DA, Bannantine JP, Fry LM, Hulubei V, De Matteis G, Park KT, Minesso S, Davis WC, Donofrio G (2024) Vaccination of cattle with a virus vector vaccine against a major membrane protein of *Mycobacterium avium* subsp. *paratuberculosis* elicits CD8 cytotoxic T cells that kill intracellular bacteria. Vet Immunol Immunopathol 275:110814
17. Kravitz A, Pelzer K, Sriranganathan N (2021) The paratuberculosis paradigm examined: a review of host genetic resistance and innate immune fitness in *Mycobacterium avium* subsp. *paratuberculosis* infection. Front Vet Sci 8:721706
18. Jolly A, Lompardía S, Hajos SE, Mundo SL (2016) Evidence of a pro-apoptotic effect of specific antibodies in a bovine macrophage model of infection with *Mycobacterium avium* subsp. *paratuberculosis*. Vet Immunol Immunopathol 169:47–53
19. Johansen MD, de Silva K, Plain KM, Whittington RJ, Purdie AC (2019) *Mycobacterium avium* subspecies *paratuberculosis* is able to manipulate host lipid metabolism and accumulate cholesterol within macrophages. Microb Pathog 130:44–53
20. Berger ST, Griffin FT (2006) A comparison of ovine monocyte-derived macrophage function following infection with *Mycobacterium avium* ssp. *avium* and *Mycobacterium avium* ssp. *paratuberculosis*. Immunol Cell Biol 84:349–356
21. Arteche-Villasol N, Gutiérrez-Expósito D, Vallejo R, Espinosa J, Elguezabal N, Ladero-Auñon I, Royo M, Ferreras MC, Benavides J, Pérez V (2021) Early response of monocyte-derived macrophages from vaccinated and non-vaccinated goats against in vitro infection with *Mycobacterium avium* subsp. *paratuberculosis*. Vet Res 52:69
22. Arsenault RJ, Maattanen P, Daigle J, Potter A, Griebel P, Napper S (2014) From mouth to macrophage: mechanisms of innate immune subversion by *Mycobacterium avium* subsp. *paratuberculosis*. Vet Res 45:54
23. Jolly A, Fernández B, Mundo SL, Elguezabal N (2023) Modeling paratuberculosis in laboratory animals, cells, or tissues: a focus on their applications for pathogenesis, diagnosis, vaccines, and therapy studies. Animals 13:3553
24. Coussens PM (2001) *Mycobacterium paratuberculosis* and the bovine immune system. Anim Health Res Rev 2:141–162
25. de Silva K, Plain K, Purdie A, Begg D, Whittington R (2018) Defining resilience to mycobacterial disease: characteristics of survivors of ovine paratuberculosis. Vet Immunol Immunopathol 195:56–64
26. Zapico D, Espinosa J, Muñoz M, Reyes LE, Benavides J, García Marín JF, Fernández M (2025) Influence of paratuberculosis vaccination on the local immune response in experimentally infected calves: an immunohistochemical analysis. Animals (Basel) 15:1841
27. Ochando J, Mulder WJM, Madsen JC, Netea MG, Duivenvoorden R (2023) Trained immunity—basic concepts and contributions to immunopathology. Nat Rev Nephrol 19:23–37
28. Dominguez-Andres J, Netea MG (2019) Long-term reprogramming of the innate immune system. J Leukoc Biol 105:329–338
29. Kopp F, Mendell JT (2018) Functional classification and experimental dissection of long noncoding RNAs. Cell 172:393–407
30. Gao Y, Cao J, Han B, Sun D (2025) Preliminary exploration of mRNA, lncRNA, and miRNA expressions in the bovine jejunum unveils novel aspects of *Mycobacterium avium* subspecies paratuberculosis infections. BMC Genomics 26:108
31. Badia-Bringué G, Asselstine V, Cánovas Á, Alonso-Hearn M (2025) Genome-wide long non-coding RNA expression profile and its regulatory role in the ileocecal valve from *Mycobacterium avium* subsp. *paratuberculosis*-infected cattle. Front Vet Sci 12:1601267
32. Gupta P, Peter S, Jung M, Lewin A, Hemmrich-Stanisak G, Franke A, von Kleist M, Schütte C, Einspanier R, Sharbati S, zur Bruegge J (2019) Analysis of long non-coding RNA and mRNA expression in bovine macrophages brings up novel aspects of *Mycobacterium avium* subspecies *paratuberculosis* infections. Sci Rep 9:1571
33. Marete A, Ariel O, Ibeagha-Awemu E, Bissonnette N (2021) Identification of long non-coding RNA isolated from naturally infected macrophages and associated with bovine Johne's disease in Canadian Holstein using a combination of neural networks and logistic regression. Front Vet Sci 8:639053
34. Bao Y, Wu S, Yang T, Wang Z, Wang Y, Jiang X, Ma H (2022) Analysis of long non-coding RNA expression profile of bovine monocyte-macrophage infected by *Mycobacterium avium* subsp. *paratuberculosis*. BMC Genomics 23:768
35. Oyanguren M, Molina E, Mugica M, Ladero-Auñon I, Fuertes M, Fernández M, Benavides J, Elguezabal N (2024) Probiotic bacteria can modulate

immune responses to paratuberculosis vaccination. Front Cell Infect Microbiol 14:1394070
36. Arteche-Villasol N, Benavides J, Espinosa J, Vallejo R, Royo M, Ferreras MdelC, Ferreras MC, Pérez V, Gutiérrez-Expósito D (2020) Optimized in vitro isolation of different subpopulation of immune cells from peripheral blood and comparative techniques for generation of monocyte-derived macrophages in small ruminants. Vet Immunol Immunopathol 230:110131
37. Ladero-Auñon I, Molina E, Holder A, Kolakowski J, Harris H, Urkitza A, Anguita J, Werling D, Elguezabal N (2021) Bovine neutrophils release extracellular traps and cooperate with macrophages in *Mycobacterium avium* subsp. *paratuberculosis* clearance in vitro. Front Immunol 12:645304
38. Wright MW (2014) A short guide to long non-coding RNA gene nomenclature. Hum Genomics 8:7
39. Bao Z, Yang Z, Huang Z, Zhou Y, Cui Q, Dong D (2019) LncRNADisease 2.0: an updated database of long non-coding RNA-associated diseases. Nucleic Acids Res 47:D1034–D1037
40. Yu G, Wang LG, Han Y, He QY (2012) ClusterProfiler: an R package for comparing biological themes among gene clusters. OMICS 16:284–287
41. Sajiki Y, Konnai S, Nagata R, Kawaji S, Nakamura H, Fujisawa S, Okagawa T, Maekawa N, Kato Y, Suzuki Y, Murata S, Mori Y, Ohashi K (2021) The enhancement of Th1 immune response by anti-PD-L1 antibody in cattle infected with *Mycobacterium avium* subsp. *paratuberculosis*. J Vet Med Sci 83:162–166
42. Reddacliff L, Eppleston J, Windsor P, Whittington R, Jones S (2006) Efficacy of a killed vaccine for the control of paratuberculosis in Australian sheep flocks. Vet Microbiol 115:77–90
43. Weiss DJ, Evanson OA, Moritz A, Deng MQ, Abrahamsen MS (2002) Differential responses of bovine macrophages to *Mycobacterium avium* subsp. *paratuberculosis* and *Mycobacterium avium* subsp. *avium*. Infect Immun 70:5556–5561
44. Mosovsky K, Silva E, Troyer R, Propst-Graham K, Dow S (2014) Interaction of interferon gamma-induced reactive oxygen species with ceftazidime leads to synergistic killing of intracellular *Burkholderia pseudomallei*. Antimicrob Agents Chemother 58:5954–5963
45. Ben-Khemis M, Liu D, Pintard C, Song Z, Hurtado-Nedelec M, Marie JC, El-Benna J, Dang PM (2023) TNFα counteracts interleukin-10 anti-inflammatory pathway through the NOX2-Lyn-SHP-1 axis in human monocytes. Redox Biol 67:102898
46. Lendemans S, Rani M, Selbach C, Kreuzfelder E, Schade FU, Flohé S (2006) GM-CSF priming of human monocytes is dependent on ERK1/2 activation. J Endotoxin Res 12:10–20
47. Gurung RB, Purdie AC, Whittington RJ, Begg DJ (2014) Cellular and humoral immune responses in sheep vaccinated with candidate antigens MAP2698c and MAP3567 from *Mycobacterium avium* subspecies *paratuberculosis*. Front Cell Infect Microbiol 4:93
48. van Schaik G, Stehman SM, Jacobson RH, Schukken YH, Shin SJ, Lein DH (2005) Cow-level evaluation of a kinetics ELISA with multiple cutoff values to detect fecal shedding of *Mycobacterium avium* subspecies *paratuberculosis* in New York State dairy cows. Prev Vet Med 72:221–236
49. Santema W, Rutten V, Koets A (2011) Bovine paratuberculosis: recent advances in vaccine development. Vet Q 31:183–191
50. Italiani P, Boraschi D (2014) From monocytes to M1/M2 macrophages: phenotypical vs. functional differentiation. Front Immunol 5:514
51. Jungi TW, Hafner S (1986) Quantitative assessment of Fc receptor expression and function during in vitro differentiation of human monocytes to macrophages. Immunology 58:131–137
52. Schulert GS, Allen LAH (2006) Differential infection of mononuclear phagocytes by *Francisella tularensis*: role of the macrophage mannose receptor. J Leukoc Biol 80:563–571
53. Chen T, Blanc C, Eder AZ, Prados-Rosales R, Souza ACO, Kim RS, Glatman-Freedman A, Joe M, Bai Y, Lowary TL, Tanner R, Brennan MJ, Fletcher HA, McShane H, Casadevall A, Achkar JM (2016) Association of human antibodies to arabinomannan with enhanced mycobacterial opsonophagocytosis and intracellular growth reduction. J Infect Dis 214:300–310
54. Purdie AC, Plain KM, Pooley H, Begg DJ, de Silva K, Whittington RJ (2022) Correlates of vaccine protection against *Mycobacterium avium* subspecies *paratuberculosis* infection revealed in a transcriptomic study of responses in Gudair® vaccinated sheep. Front Vet Sci 9:1004237
55. Moorlag SJCFM, Rodriguez-Rosales YA, Gillard J, Fanucchi S, Theunissen K, Novakovic B, de Bont CM, Negishi Y, Fok ET, Kalafati L, Verginis P, Mourits VP, Koeken VACM, de Bree LCJ, Pruijn GJM, Fenwick C, van Crevel R, Joosten LAB, Joosten I, Koenen H, Mhlanga MM, Diavatopoulos DA, Chavakis T, Netea MG (2020) BCG vaccination induces long-term functional reprogramming of human neutrophils. Cell Rep 33:108387
56. Walther K, Schulte LN (2021) The role of lncRNAs in innate immunity and inflammation. RNA Biol 18:587–603
57. Bilbao-Arribas M, Varela-Martínez E, Abendaño N, de Andrés D, Luján L, Jugo BM (2021) Identification of sheep lncRNAs related to the immune response to vaccines and aluminium adjuvants. BMC Genomics 22:770
58. Liang S, Ma J, Gong H, Shao J, Li J, Zhan Y, Wang Z, Wang C, Li W (2022) Immune regulation and emerging roles of noncoding RNAs in *Mycobacterium tuberculosis* infection. Front Immunol 13:987018
59. Niedergang F, Colucci-Guyon E, Dubois T, Raposo G, Chavrier P (2003) ADP ribosylation factor 6 is activated and controls membrane delivery during phagocytosis in macrophages. J Cell Biol 161:1143–1150
60. Jiang C, Ma N, Cao H, Zeng W, Ren J, Hu Y, Zhou J, Zhang M, Li C, Lang Y, Li W, He Q (2022) TurboID screening of the OmpP2 protein reveals host proteins involved in recognition and phagocytosis of *Glaesserella parasuis* by iPAM cells. Microbiol Spectr 10:e0230722
61. Kuehnel MP, Goethe R, Habermann A, Mueller E, Rohde M, Griffiths G, Valentin-Weigand P (2001) Characterization of the intracellular survival of *Mycobacterium avium* ssp. *paratuberculosis*: phagosomal pH and fusogenicity in J774 macrophages compared with other mycobacteria. Cell Microbiol 3:551–566
62. Shao S, Brown A, Santhanam B, Hegde RS (2015) Structure and assembly pathway of the ribosome quality control complex. Mol Cell 57:433–444
63. Scott DC, Chittori S, Purser N, King MT, Maiwald SA, Churion K, Nourse A, Lee C, Paulo JA, Miller DJ, Elledge SJ, Harper JW, Kleiger G, Schulman BA (2024) Structural basis for C-degron selectivity across KLHDCX family E3 ubiquitin ligases. Nat Commun 15:9899
64. Lee SW, Wu LSH, Huang GM, Huang KY, Lee TY, Weng JTY (2016) Gene expression profiling identifies candidate biomarkers for active and latent tuberculosis. BMC Bioinformatics 17(Suppl 1):3
65. Sun HM, Chen XL, Chen XJ, Liu J, Ma L, Wu HY, Huang QH, Xi XD, Yin T, Zhu J, Chen Z, Chen SJ (2017) PALLD regulates phagocytosis by enabling timely actin polymerization and depolymerization. J Immunol 199:1817–1826
66. Barger SR, Vorselen D, Gauthier NC, Theriot JA, Krendel M (2022) F-actin organization and target constriction during primary macrophage phagocytosis is balanced by competing activity of myosin-I and myosin-II. Mol Biol Cell 33:br24
67. Duffy FJ, Olson GS, Gold ES, Jahn A, Aderem A, Aitchison JD, Rothchild AC, Diercks AH, Nemeth J (2022) Use of a contained *Mycobacterium tuberculosis* mouse infection model to predict active disease and containment in humans. J Infect Dis 225:1832–1840
68. Venkatesan R, Sah-Teli SK, Awoniyi LO, Jiang G, Prus P, Kastaniotis AJ, Hiltunen JK, Wierenga RK, Chen Z (2014) Insights into mitochondrial fatty acid synthesis from the structure of heterotetrameric 3-ketoacyl-ACP reductase/3R-hydroxyacyl-CoA dehydrogenase. Nat Commun 5:4805
69. Wang M, Bissonnette N, Dudemaine PL, Ibeagha-Awemu EM (2026) MicroRNA dysregulation in cow's jejunum, jejunal lymph node, and caecal Peyer's patch during *Mycobacterium avium* subsp. *paratuberculosis* infection. BMC Genomics 27:25
70. Lee JH, Park HT, Shim S, Kim S, Woo SH, Kim DY, Yoo HS (2023) Immunopathological mechanisms in the early stage of *Mycobacterium avium* subsp. *paratuberculosis* infection via different administration routes in a murine model. PLoS One 18:e0281880
71. Thom RE, Elmore MJ, Williams A, Andrews SC, Drobniewski F, Marsh PD, Tree JA (2012) The expression of ferritin, lactoferrin, transferrin receptor and solute carrier family 11A1 in the host response to BCG vaccination and *Mycobacterium tuberculosis* challenge. Vaccine 30:3159–3168
72. Deng L, Feng J, Broaddus RR (2010) The novel estrogen-induced gene EIG121 regulates autophagy and promotes cell survival under stress. Cell Death Dis 1:e32
73. Alonso-Hearn M, Canive M, Blanco-Vazquez C, Torremocha R, Balseiro A, Amado J, Varela-Martinez E, Ramos R, Jugo BM, Casais R (2019) RNA-Seq analysis of ileocecal valve and peripheral blood from Holstein cattle infected with *Mycobacterium avium* subsp. *paratuberculosis* revealed dysregulation of the CXCL8/IL8 signaling pathway. Sci Rep 9:14845

74. Lee K, Nguyen DT, Choi M, Cha SY, Kim JH, Dadi H, Seo HG, Seo K, Chun T, Park C (2013) Analysis of cattle olfactory subgenome: the first detail study on the characteristics of the complete olfactory receptor repertoire of a ruminant. BMC Genomics 14:596
75. Wang X, Iyer A, Lyons AB, Körner H, Wei W (2019) Emerging roles for G-protein coupled receptors in development and activation of macrophages. Front Immunol 10:2031
76. Bhatt B, Zhu H, Patel N, Singh N (2020) Role of G-protein coupled receptors in chemotaxis of innate lymphoid cells. Methods Mol Biol 2121:93–98
77. Orecchioni M, Kobiyama K, Winkels H, Ghosheh Y, McArdle S, Mikulski Z, Kiosses WB, Fan Z, Wen L, Jung Y, Roy P, Ali AJ, Miyamoto Y, Mangan M, Makings J, Wang Z, Denn A, Vallejo J, Owens M, Durant CP, Braumann S, Mader N, Li L, Matsunami H, Eckmann L, Latz E, Wang Z, Hazen SL, Ley K (2022) Olfactory receptor 2 in vascular macrophages drives atherosclerosis by NLRP3-dependent IL-1 production. Science 375:214–221
78. Parada Venegas D, De la Fuente MK, Landskron G, González MJ, Quera R, Dijkstra G, Harmsen HJM, Faber KN, Hermoso M (2019) Short Chain Fatty Acids (SCFAs)—mediated gut epithelial and immune regulation and its relevance for inflammatory bowel diseases. Front Immunol 10:277

Publisher's note

Springer Nature remains neutral with regard to jurisdictional claims in published maps and institutional affiliations.